

OBSERVATION OF LONG-RANGE ORDER IN TRAPPED ION PLASMAS BY BRAGG SCATTERING[†]

JOSEPH N. TAN, J.J. BOLLINGER, B. JELENKOVIC*, WAYNE M. ITANO, and D.J. WINELAND
*National Institute of Standards and Technology
325 Broadway, Boulder, CO 80303*

ABSTRACT

We have detected long-range order (crystal lattices) in atomic ions confined in a Penning trap. The crystals were observed by the Bragg scattering of nearly resonant laser light at small ($1-5^\circ$) scattering angles. Long-range order was observed in approximately spherical plasmas with as few as 5×10^4 ions (plasma radius $r_o \approx 37 a_{WS}$ where a_{WS} = Wigner-Seitz radius). With 2.7×10^5 trapped ions ($r_o \approx 65 a_{WS}$), Bragg scattering patterns were obtained that were consistent with a body-centered cubic lattice.

1. Introduction

Charged particles in a trap form a realistic model of a classical one-component plasma (OCP). For example, in a Penning trap under conditions of thermal equilibrium the trapping fields provide a uniform background of opposite charge.¹ With Doppler laser-cooling on trapped ions, temperatures of a few millikelvins can be obtained with densities greater than 10^8 cm^{-3} which results in couplings $\Gamma = q^2 / (4\pi\epsilon_o a_{WS} k_B T) > 250$.^{2,3} Here q is the ion charge, ϵ_o is the permittivity of the vacuum, a_{WS} is the Wigner-Seitz radius, k_B is Boltzmann's constant, and T is the ion temperature. These couplings are larger than the predicted liquid-solid phase transition ($\Gamma \sim 172$)⁴ for an infinite OCP and enable trapped ion plasmas to be used to study strongly coupled one-component plasmas. However, in the trapped ion experiments to date, the boundary and relatively small size of the ion plasmas have strongly affected the observed spatial correlations. In plasmas where the smallest dimension is only a few interparticle spacings, the ions form curved shells which approximately conform with the boundary of the plasma.⁵⁻⁷ These shell structures have been observed with imaging techniques in both the Penning and rf traps.⁸⁻¹⁰

In this manuscript we describe some recent experiments on approximately spherical plasmas of up to $4.7 \times 10^5 \text{ Be}^+$ ions whose dimensions are large compared to a_{WS} . Through Bragg scattering we occasionally observe the presence of long-range order or crystal lattices in the ion plasmas. Crystal lattices have been observed in the shielded Coulomb systems of colloidal suspensions¹¹ and dusty plasmas¹². However, we believe this is the first observation¹³ of crystal lattices in a pure Coulomb strongly coupled plasma. We use the

[†]Work of the US Government; not subject to US copyright

*On leave from the Institute of Physics, University of Belgrade, Yugoslavia

Penning trap in this work because it permits dimensionally large plasmas to be laser-cooled. The Penning trap¹⁴ uses a uniform, static magnetic field to confine ions in directions perpendicular to the magnetic field. A static electric field is used to confine ions in the direction parallel to the magnetic field. Due to the axial magnetic field and the radial electric field in a Penning trap, the ion plasma rotates about the magnetic field axis of the trap. The plasma rotation makes it difficult to directly image the ions in a crystal. However, Bragg scattering can still be used to observe the crystals. In the final section of this manuscript we also discuss a time-resolved experiment where the Bragg scattering signal is used to measure the plasma rotation frequency.

In an infinite, homogeneous one-component plasma, the body-centered cubic (bcc), face-centered cubic (fcc), and hexagonal close-packed (hcp) lattices have the same Madelung energy within 1 part in 10^4 , with the bcc lattice the energetically favored configuration.¹⁵ For a finite system, the surface energy and details of the boundary also determine the energetically favored configuration. Dubin¹⁶ considered a zero-temperature model which was infinite and homogeneous in two dimensions but bounded and confined in the third direction by a quadratic potential. He found that if the system was greater than ~ 60 lattice planes (in the bounded direction), a bcc-like structure was the minimum energy configuration. However, with less than 60 lattice planes the minimum energy configuration depended sensitively on the exact number of lattice planes. This calculation indicates that a trapped ion plasma may need to be larger than 60 lattice spacings along its smallest dimension to exhibit behavior which is not strongly influenced by the plasma boundary. A different analytical method developed by Hasse gives a comparable prediction.¹⁷ With a spacing of $\sim 1.5a_{ws}$ between typical low order lattice planes,¹⁶ a spherical plasma with a diameter of $60 \times 1.5a_{ws}$ consists of $\sim 9 \times 10^4$ ions. We have observed long-range order (crystals) in approximately spherical plasmas with greater than 5×10^4 ions. With 2.7×10^5 ions, the observed Bragg scattering pattern was predominantly consistent with a bcc lattice, the expected infinite volume structure.

2. Experimental Set-up

Figure 1 shows a sketch of our experimental set-up. The Penning trap is formed by a 127 mm stack of cylindrical electrodes with 40.6 mm inner diameter, in a 10^{-8} Pa vacuum (133 Pa = 1 Torr). A superconductive magnet provides a uniform magnetic field ($B_0=4.5$ T) parallel to the symmetry axis (${}^9\text{Be}^+$ cyclotron frequency of $\Omega/2\pi=qB_0/m=7.55$ MHz, where m is the ion mass). The static electric field is generated by applying $V_0=1$ kV between the end and central electrodes of the trap (a single ion oscillates at $\omega_z/2\pi=795$ kHz).

The trapped ${}^9\text{Be}^+$ ions are laser-cooled and optically pumped into the $2s^2S_{1/2}(M_I=-3/2, M_J=-1/2)$ state by tuning the laser frequency ($\lambda \approx 313$ nm) slightly below the $2s^2S_{1/2}(-3/2, -1/2) \rightarrow 2p^2P_{3/2}(-3/2, -3/2)$ resonance frequency.^{2,18} A laser-cooled ion plasma in thermal

equilibrium forms a uniform density plasma (number density n_0) with sharp boundaries. In a Penning trap with quadratic potential ($\Phi = m\omega_z^2[2z^2-r^2]/[2q]$) and in which image charge effects from the trap electrodes are negligible, the boundary is a spheroid given by $(x^2+y^2)/r_s^2 + z^2/z_s^2 = 1$ (for a spherical plasma $r_s=z_s\equiv r_0$). The residual thermal motions of the ions are superimposed upon a rigid rotation of the plasma about the magnetic field axis (z-axis) at a frequency ω_r . The aspect ratio $\alpha\equiv z_s/r_s$ of the spheroid varies with ω_r .^{18,19} A laser beam directed normal to the z-axis (not shown in

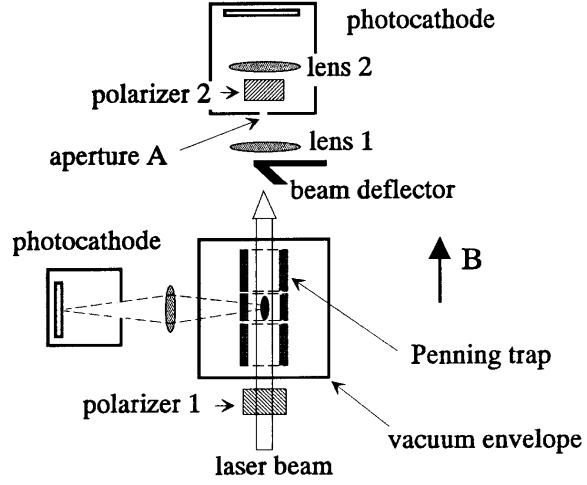


Figure 1. Schematic diagram (not to scale) of the experimental set-up for detection of the Bragg scattering as described in the text.

Fig. 1 and turned off during the Bragg scattering) can exert a torque that changes ω_r within $40.8 \text{ kHz} < \omega_r/(2\pi) < 7.51 \text{ MHz}$, thus controlling the shape and density of the plasma.¹⁹ An $f/5$ imaging system along an axis perpendicular to the z-axis, with a laser beam along the z-axis (beam waist $\sim 0.4 \text{ mm}$, power $\sim 200 \mu\text{W}$), gives a side-view image of the ion plasma, thus monitoring z_s and r_s , which, in turn, yield α , ω_r , n_0 , a_{WS} , and the number N of trapped ions.¹⁹ Typical values for these parameters in the work described here are $\alpha \sim 1$, $\omega_r/(2\pi) \sim 125 \text{ kHz}$, $n_0 \sim 4 \times 10^8$, $a_{\text{WS}} \sim 8.4 \mu\text{m}$. (The measurement of ω_r and therefore most of these parameters is significantly improved by an autocorrelation measurement of the Bragg-scattered light described in the last section.)

The laser beam along the z-axis in Fig. 1 is used both to laser-cool the ions and also to perform the Bragg scattering. Because $\lambda/a_{\text{WS}} \sim 0.04$, the diffraction pattern occurs at small angles (a few degrees) relative to the initial beam direction. The main purpose of the Bragg scattering apparatus in Fig. 1 is to detect the light scattered at small angles by the ions while hiding from the forward-scattered light from the vacuum windows. The incident laser beam ($\mathbf{k}_i = 2\pi\mathbf{z}/\lambda$) first passes through linear polarizer 1, and then into the vacuum chamber. Upon exiting the ion trap, the laser beam is diverted away from the detector by a set of mirrors. The photons scattered by the ions ($\mathbf{k}_s = (2\pi/\lambda)\mathbf{k}_s$) are collected by lens 1 ($f=19 \text{ cm}$, $z=25.5 \text{ cm}$ from the ions), forming an image of the ions at a small aperture (A) to reduce the background. The diffraction pattern is then relayed by lens 2 ($f \approx 24 \text{ cm}$) to the photocathode of a photon-counting imaging tube ($z \approx 160 \text{ cm}$). Linear polarizer 2 is inserted after the aperture. The polarization axes of polarizers 1 and 2 are crossed to attenuate, with extinction ratio $> 10^5$, stray light which leaks through the small aperture and has the same polarization as polarizer 1. The photons from the ions are attenuated by only a factor of 2 since they are mainly circularly polarized. The angular acceptance of the system is limited by lens 1 to be $\pm 5.4^\circ$. For plasmas of a few hundred thousand ions, the ion fluorescence is strong enough that it was

necessary to insert a 10-20 dB attenuator in front of the photon-counting imaging tube.

3. Bragg Scattering Results

The following procedure was typically used in obtaining a Bragg scattering pattern. First, the perpendicular (to the z-axis) laser beam was used to set the density and aspect ratio of the cloud. Typical densities were $n_0 \sim 4 \times 10^8 \text{ cm}^{-3}$ with aspect ratios close to spherical (between 0.5 and 2). The perpendicular beam was then blocked and the parallel beam unblocked with its frequency well below atomic resonance where little scattering takes place. The frequency of the parallel beam was then increased to near resonance and a Bragg scattering pattern was recorded. The laser frequency was then detuned and increased again (or perhaps the laser was blocked and then unblocked) and another pattern was recorded. The expansion of the plasma was slow enough that this process could be repeated many times before the perpendicular beam was used to reset the plasma density and aspect ratio. On some occasions we observed Bragg scattering patterns that consisted of several sharp rings such as shown in Fig. 2a. Patterns like this with up to 9 narrow rings were observed with as few as $N \approx 6 \times 10^4$ trapped ions. The circular intensity maxima in Fig. 2a are Bragg peaks. The radius of a Bragg peak is inversely proportional to a_{WS} , a fact which was verified by changing the Wigner-Seitz radius using laser torque. Figure 2b is a differential scattering cross section generated from Fig. 2a by averaging the photon counts azimuthally about the z-axis (the laser beam axis which is normal to the figure). Figure 2b is qualitatively different from the static structure factor $S(q)$ in Fig. 2c for the quenched OCP fluid and shell structure,²⁰ both of which exhibit short range order characteristic of a fluid. Here $q = |\mathbf{k}_i - \mathbf{k}_s| = (4\pi/\lambda)\sin(\theta/2)$ where θ is the scattering angle. The fluid-like patterns have only one strong narrow peak. In contrast, Fig. 2b has 4 narrow peaks which indicate the formation of a crystal lattice. As mentioned earlier, such long-range order was not observed every time we cooled an ion plasma. We have not determined whether this was because a crystal had not formed or a crystal had formed but was not observed (because, for example, the crystal orientation did not produce Bragg peaks).

In order to compare the Bragg peak positions with the calculated positions for the bcc, fcc and hcp lattices, the radii of the Bragg rings must be calibrated in terms of the scattering angle. This was done for a set of 14 diffraction patterns which were obtained on a plasma of 2.7×10^5 ions. For each pattern, a_{WS} was determined with about 5% uncertainty from the measured α . Figure 3a shows a histogram of the number of observed Bragg peaks as a function of qa_{WS} . For $qa_{\text{WS}} < 10$, the histogram shows 5 groups of peaks. These groups are consistent with a bcc lattice but not an fcc lattice. (They are also nominally consistent with a subset of hcp peaks, but if many hcp crystals were forming randomly, we would expect to see more groups or at least broader groups of peaks.)

Comparison of the groups of peaks with different calculated Bragg peaks for $qa_{ws} > 10$ is limited by the uncertainty in the determination of a_{ws} . However, if a_{ws} is determined by fitting

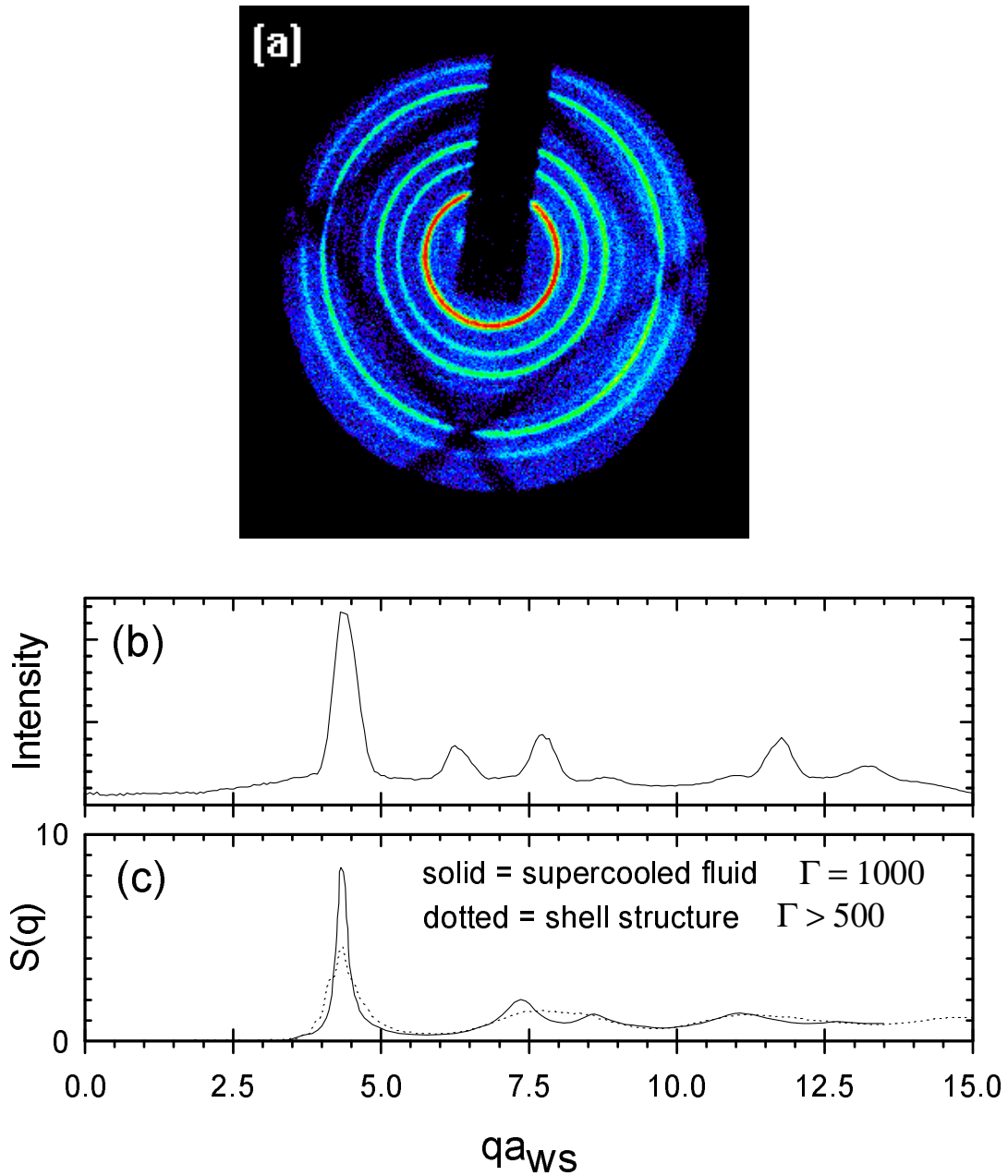


Figure 2. (a) Bragg scattering pattern observed from 2.7×10^5 ions showing the presence of a crystal(s). The diffraction pattern is partially blocked by a rectangular shadow due to the laser beam deflector and a square shadow due to a wire mesh. (b) Differential cross-section obtained from an azimuthal average of (a) about the z-axis. © Fluid-like $S(q)$ calculated for a super-cooled OCP and an $N=5 \times 10^3$ ion cloud with shells.²⁰

each diffraction pattern used in Fig. 3a to the calculated bcc peaks, we see from Fig. 3b that with 2.7×10^5 trapped ions the Bragg peaks are consistent with a bcc lattice even as far as $qa_{ws} \sim 14$.

A lower limit on the size of the ion crystals can be obtained from the widths of the Bragg peaks as observed in Fig. 2b. A crystal with dimension L has a Bragg-peak width of $\Delta \sim \lambda/L$, where Δ is the angular FWHM of the Bragg peak. We find that, on average, $\Delta \sim 2$ mrad, which gives $L \sim 150 \mu\text{m}$ ($\sim 20a_{ws}$) and a few thousand ions per crystal. This is a lower limit, since the observed widths could be instrumentally broadened. The negligible change measured in Δ with N supports such broadening. In addition, the intensity in the Bragg peaks increased with N , which indicates that the crystal size is growing with the number of trapped ions. The crystallized region is probably surrounded by at least ~ 20 shells (based on a simulation with 2×10^4 ions).²¹ For a plasma with 2.7×10^5 ions, this corresponds to about 2.3×10^5 ions or a large fraction of the total plasma in these boundary shell layers. The positions of these ions are correlated only over a few interparticle spacings and may be the source of the background signal in Fig. 2b. If the peaks in Fig. 2b are due to Bragg scattering off a single crystal, we estimate that the crystal must contain $\sim 10^4$ ions in order to produce peak intensities greater than the uncorrelated background due to 2.3×10^5 ions.

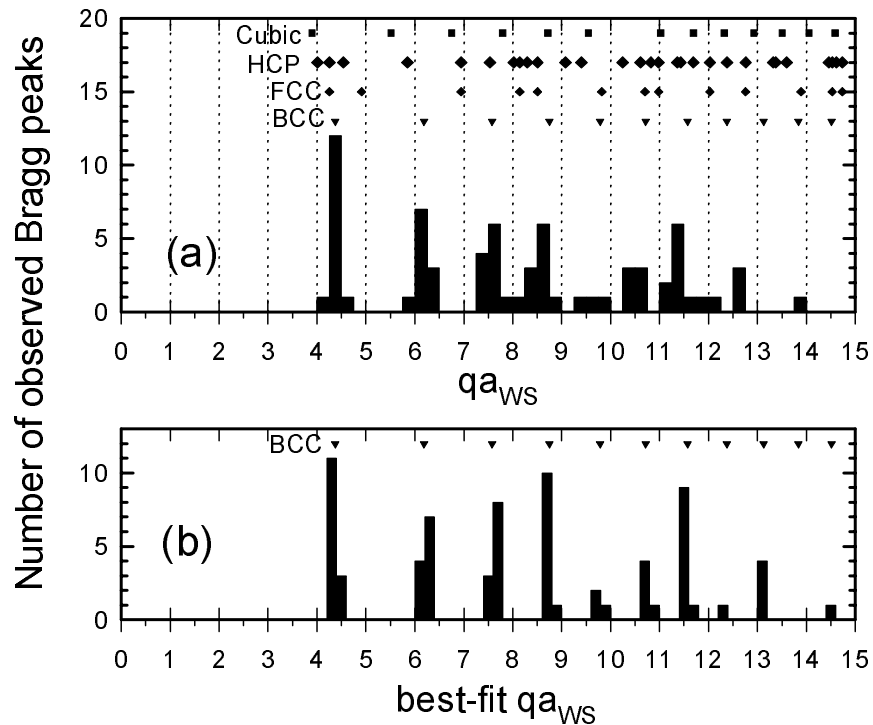


Figure 3. The number of observed peaks (not intensity) from 14 diffraction patterns with $N=2.7 \times 10^5$ ions. In (a) there are no adjustable parameters (a_{ws} is determined from the observed α). In (b), a_{ws} is determined by fitting the diffraction patterns used in (a) to a bcc lattice. The ticks indicate the location of Bragg peaks for the simple cubic, hcp, fcc, and bcc lattices.

4. Time-Resolved Experiments

The Bragg scattering pattern from a single, stationary crystal consists of dots (a Laue pattern). In our experiment the crystal rotates ($\omega_r/(2\pi) \approx 125$ kHz) about the magnetic field axis (which is aligned with the laser beam axis to within 0.5°). This rotation turns the Laue pattern of dots into rings. At any given point on a ring, the light intensity should be modulated at the rotation frequency or a multiple of the rotation frequency if the ring consists of more than one dot. The experimental set-up in Fig. 1 was modified to look for a time dependence of the Bragg-scattered light. The camera in Fig. 1 was replaced with a mirror which made a 45° angle with respect to the laser beam axis (the z-axis). The mirror had a small hole drilled parallel to the z-axis which could be positioned on one of the Bragg rings. The light which passed through this hole was detected by a photomultiplier tube. A pulse from the photomultiplier triggered a multichannel scaler. The multichannel scaler then measured the arrival times of photomultiplier pulses for ~ 0.5 ms after the trigger. The Bragg scattering pattern reflected from the 45° mirror was re-imaged onto the camera.

Figure 4a shows an example of an autocorrelation pattern obtained on the first ring from a plasma of 4.7×10^5 trapped ions. The pattern indicates that the ring consists of 4 equally spaced dots of unequal intensity. From the side-view image of the plasma, $2\pi/\omega_r$ is determined within $\sim 15\%$, which unambiguously identifies the period of the autocorrelation pattern. However, a strong autocorrelation signal can be used to improve the measurement of ω_r to $\sim 0.1\%$ with less than 10 s of averaging. The output of the phototube was also used to "trigger" the camera recording the Bragg-scattered light. A pulse from the phototube would enable the position of a photon to be recorded if it arrived within a window (duration much less than $2\pi/\omega_r$) that was a fixed delay after the photomultiplier pulse. Figure 4b shows the gated image that was recorded simultaneously with the autocorrelation pattern in Fig. 4a. The gated Laue pattern provides more information for determining the crystal type and the crystal orientation relative to the laser beam. So far most, but not all, of the Laue patterns we have observed are consistent with a single crystal.

The data in Fig. 4 can be understood as Bragg scattering off a single bcc or fcc crystal as follows. First, Bragg scattering is observed at small ($1-5^\circ$) scattering angles. This means that the planes which give rise to Bragg-scattered light are nearly vertical (parallel to the z-axis). Second, a Bragg ring with momentum transfer q will persist over an angular change in crystal orientation of $\sim (2\pi/L)/q$. For low-order planes, $q \sim (2\pi/a)$, where a is the lattice constant ($a[\text{bcc}] = 2.03a_{\text{WS}}$; $a[\text{fcc}] = 2.56a_{\text{WS}}$). For our small crystals, this means the crystal can be tilted with respect to the z-axis over a range $a/L \sim 0.1$ rad or 5° and still give rise to the same Bragg peak. This means a low order, nearly vertical plane will produce two Laue dots separated by 180° . The four equally spaced dots making up the first Bragg ring in Fig. 4 are therefore produced by two vertical planes which are 90° from each other. This rules out the hcp lattice as a possibility; however the planes could be bcc 110 planes or fcc 200 planes where the laser beam is approximately aligned with a 4-fold symmetry axis of the cubic cell. The rest of the Laue pattern in Fig. 4b is consistent with this interpretation. To distinguish between bcc and fcc in this case, an absolute angular calibration of the rings must be done.

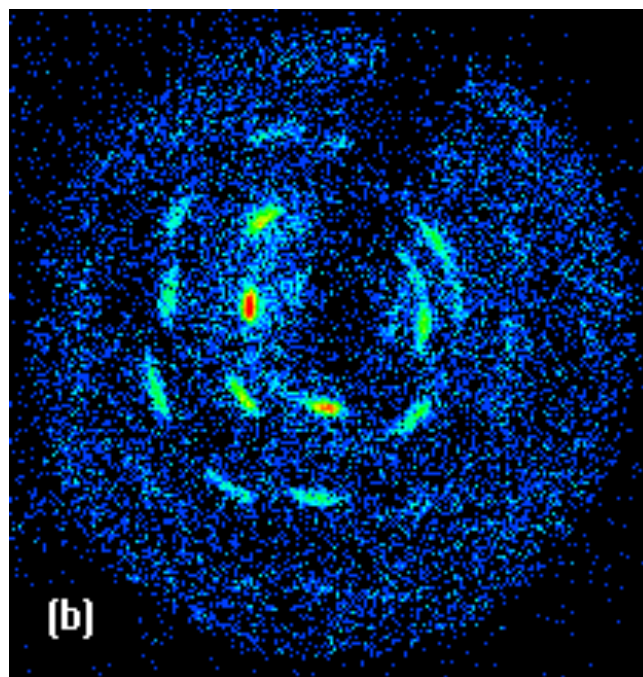
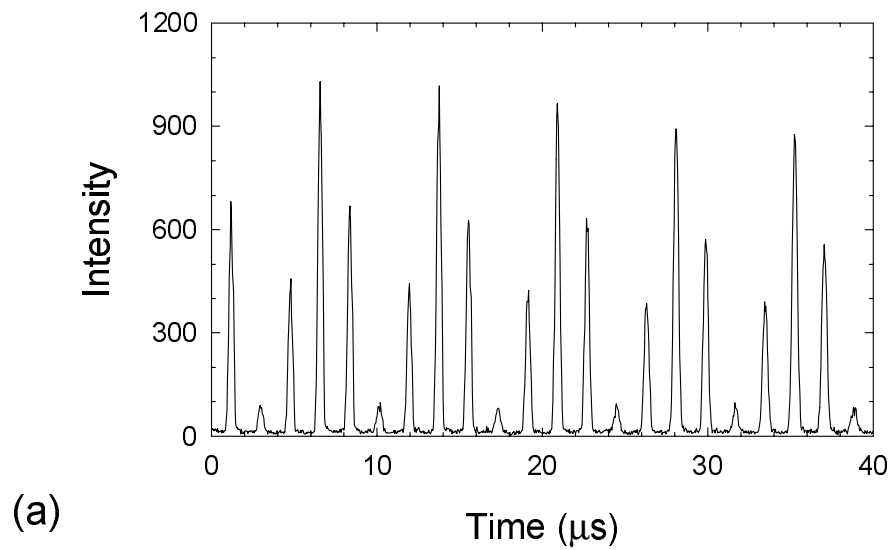


Figure 4. (a) Autocorrelation pattern and (b) gated image simultaneously obtained on 4.7×10^5 trapped ions. The photomultiplier tube was sampling counts from the first ring.

We are doing this with the time resolved set-up as well as analyzing other Laue patterns. This will enable us to check with increased confidence that the lattice most frequently formed with a few hundred thousand trapped ions is bcc.

5. Acknowledgments

We gratefully acknowledge the support of the US Office of Naval Research. We acknowledge stimulating discussions with D.H.E. Dubin, J.P. Schiffer, H.E. DeWitt, and S. Ichimaru. We thank J.P. Schiffer for providing simulation data of shell structure, D.H.E. Dubin for providing calculations of $S(q)$ from shells and OCP fluids, and S. Ichimaru for permission to reproduce $S(q)$ for the supercooled OCP fluid (Fig. 2c). We also thank D. Berkeland, F. Cruz, and M. Young for carefully reading the manuscript.

6. References

1. J.H. Malmberg and T.M. O'Neil, *Phys. Rev. Lett.* **39** (1977) 1333.
2. J.J. Bollinger and D.J. Wineland, *Phys. Rev. Lett.* **53** (1984) 348.
3. J.J. Bollinger, D.J. Wineland, and D.H.E. Dubin, *Phys. Plasmas* **1** (1994) 1403.
4. E.L. Pollock and J.P. Hansen, *Phys. Rev.* **A8** (1973) 3110; W.L. Slattery, G.D. Doolen, and H.E. DeWitt, *Phys. Rev.* **A26** (1982) 2255; S. Ogata and S. Ichimaru, *Phys. Rev.* **A36** (1987) 5451; D.H.E. Dubin, *Phys. Rev.* **A42** (1990) 4972.
5. A. Rahman and J.P. Schiffer, *Phys. Rev. Lett.* **57** (1986) 1133.
6. H. Totsuji, in *Strongly Coupled Plasma Physics*, ed. F.J. Rogers and H.E. Dewitt (Plenum, New York, 1987) p. 19.
7. D.H.E. Dubin and T.M. O'Neil, *Phys. Rev. Lett.* **60** (1988) 511.
8. S.L. Gilbert, J.J. Bollinger, and D.J. Wineland, *Phys. Rev. Lett.* **60** (1988) 2022.
9. G. Birkl, S. Kassner, and H. Walther, *Nature* **357** (1992) 310.
10. R.F. Wuerker, H. Shelton, and R.V. Langmuir, *J. Appl. Phys.* **30** (1959) 342; F. Diedrich, E. Peik, J.M. Chen, W. Quint, and H. Walther, *Phys. Rev. Lett.* **59** (1987) 2931; D.J. Wineland, J.C. Bergquist, W.M. Itano, J.J. Bollinger, and C.H. Manney, *Phys. Rev. Lett.* **59** (1987) 2935; Th. Sauter, H. Gilhaus, W. Neuhauser, R. Blatt, and P. Toschek, *Europhys. Lett.* **7** (1988) 317.
11. N.A. Clark, A.J. Hurd, and B.J. Ackerson, *Nature* **281** (1979) 57; C.A. Murray and D.G. Grier, *Amer. Sci.* **83** (1995) 238; L.B. Chen, C.F. Zukoski, B.J. Ackerson, H.J.M. Hanley, G.C. Straty, J. Barker and C.J. Glinka, *Phys. Rev. Lett.* **69** (1992) 688.
12. J.H. Chu and Lin I, *Phys. Rev. Lett.* **72** (1994) 4009; H. Thomas, G.E. Morfill, V. Demmel, and J. Goree, *Phys. Rev. Lett.* **73** (1994) 652.
13. Preliminary results are in J.N. Tan, J.J. Bollinger, A.S. Barton, and D.J. Wineland, in *Non-Neutral Plasma Physics II*, ed. J. Fajans and D.H.E. Dubin (AIP Press, New York, 1995) p. 215.
14. H.G. Dehmelt, *Adv. At. Mol. Phys.* **3** (1967) 53; **5** (1969) 109.
15. S.G. Brush, H.L. Sahlin, and E. Teller, *J. Chem. Phys.* **45** (1966) 2102.
16. D.H.E. Dubin, *Phys. Rev.* **A40** (1989) 1140.
17. R.W. Hasse and V.V. Avilov, *Phys. Rev.* **A44** (1991) 4506.
18. L.R. Brewer, J.D. Prestage, J.J. Bollinger, W.M. Itano, D.J. Larson and D.J. Wineland, *Phys. Rev.* **A38** (1988) 859.

19. J.J. Bollinger, D.J. Heinzen, F.L. Moore, W.M. Itano, D.J. Wineland, and D.H.E. Dubin, *Phys. Rev.* **A48**, (1993) 525.
20. The supercooled $S(q)$, calculated for an unbounded OCP with $\Gamma=1000$, is from Fig. 6b in S. Ichimaru, H. Iyetomi, and S. Tanaka, *Phys. Rep.* **149** (1987) 91. The shell structure $S(q)$ is calculated from the simulation data, received from J.P. Schiffer, for an $N=5000$ spherical plasma with $\Gamma>500$. Similar shell $S(q)$ have been calculated by D.H.E. Dubin.
21. J.P. Schiffer, in *Non-Neutral Plasma Physics II*, ed. J. Fajans and D.H.E. Dubin (AIP Press, New York, 1995) p. 191.